ISTITUTO NAZIONALE DI FISICA NUCLEARE
Laboratori Nazionali di Frascati

ECFA/LEP Working Group
SSG/6/5/May 1979

LNF-79/40(R)
3 Luglio 1979

R. Del Fabbro and G. P. Murtas: TWO PHOTON MASS SENSITIVITY BY A TAGGING SYSTEM AT LEP SHORT INSERTION.

Servizio Documentazione
dei Laboratori Nazionali di Frascati
Cas. Postale 13 - Frascati (Roma)

ECFA/LEP Working Group
SSG/6/5/May 1979

INFN - Laboratori Nazionali di Frascati
Servizio Documentazione

LNF-79/40(R)
3 Luglio 1979

R. Del Fabbro(x) and G. P. Murtas: TWO PHOTON MASS SENSITIVITY BY A TAGGING SYSTEM AT LEP SHORT INSERTION.

1. - INTRODUCTION.

The present note is devoted to study the two photon mass sensitivity one can obtain at LEP short insertion.

The investigation of that important point of the two photon physics studies has been performed using results we have already obtained in our work(1) on the angular acceptances and efficiencies of a tagging system at LEP short insertion.

Now we look at the two photon production of a system X in the process:

$$e^+e^- \longrightarrow e^+e^-X$$

(see the corresponding Feynman graph in the Fig. 1a).

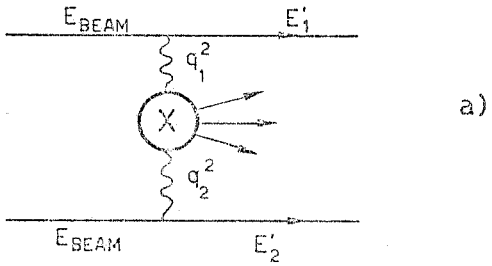

a)

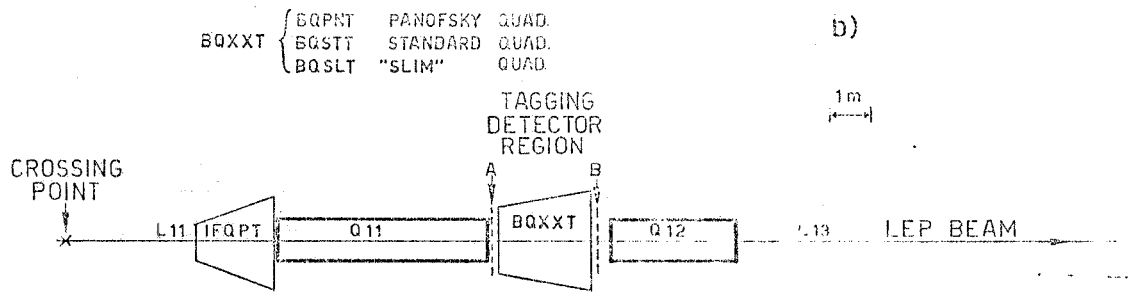

FIG. 1 - a) Feynman graph of the system X creation through two photon channel;
b) Sketch of the optical component of the LEP machine on the short insertion side.

For a fixed mass M_X and velocity β_X of the system X, the energies x_γ of two colliding photons and therefore the two corresponding electron energies x_e are also fixed.

Two parameters are left free : the two transverse fourmomenta q^2, which are tied at the recoil electron angle θ_e by the kinematical relation (holding for very small angles) :

$$\theta_e^2 = E_{beam}^{-2}\left[-q^2/x_e - (m_e x_\gamma/x_e)^2\right]$$

where m_e is the electron mass.

So in evaluating the production yield of the system X one has to perform an integration on the fourmomenta q^2 and the result depends on the electron angles accepted by the tagging system.

However in the present study we exclude the large q^2 cases (deep inelastic region) and we limit ourselves to the two "quasi real photon" collision, that allows to us to work in the Equivalent Photon Approximation frame.

So in spite to a large yield one expect at low q^2, since the cross section depends on the photon propagator factors $1/q^2$, one can observe that the low q^2 values correspond to very small electron angles just in the region where the recoil electron efficiency is suppressed.

That shows that it is necessary to know the angular acceptances and the efficiencies of a tagging system in order to evaluate the two photon mass sensitivity.

At this end in the Section 2 we have completed the work done in the ref. (1) extending our results on the electron energy region very close to 1 (from 0.9 to 0.999 times the electron beam energy).

By those results we are able to give in the Section 3 some knowledge on the two photon mass sensitivity at LEP beam energy of 80 GeV relatively to a double arm tagging system.

Also in this note we maintain three possible choices in using different solutions for the low-β quadrupole : the Panofsky quadrupole, the LEP machine standard quadrupole and the "slim" quadrupole (see for description the ref. (1)).

In fact the experimental performance relative to these possible solutions are quite different.

So for comparison we have thought of doing an useful thing showing in the Section 4 the geometry of detected electron fluxes behind the low-β quadrupole, in order to give a guess of the tagging detector shape and where and how the sensible tagging parts may be located.

2. - TAGGING EFFICIENCY FOR ELECTRON ENERGIES VERY CLOSE TO BEAM ENERGY.

Suppose to have two identical tagging detector arms set up on both side of the short insertion. We are interested to study the two photon mass sensitivity of the double tagging system in a large range of masses. For doing that we need to know correspondently the angular acceptances and the efficiencies in a large range of the recoil electron energy too.

We have already performed that study in the ref. (1) up to the electron energy $x_e = 0.9$ with good accuracy and up to 0.98 with an indetermination of the order of 20%.

However the increasing behaviour in energy of the term we had neglected didn't allow to us to reach a larger electron energy. For that reason in this section we study the angular acceptances and the efficiencies for electron energies very close to 1, i. e. in the range from 0.9 to 0.999.

Now we consider the expression of the electron flux emitted in the polar angular range from θ_{min} to θ_{max} :

$$N(x_e, \theta_{min}, \theta_{max}) = \frac{\alpha}{\pi(1-x_e)}\left[(1+x_e^2)\ln\frac{\theta_{max}}{\theta_{min}} - \frac{(1+x_e)^2}{4}\ln\frac{(1-x_e)^2+x_e\theta_{max}^2}{(1-x_e)^2+x_e\theta_{min}^2}\right] \qquad (1)$$

as we have noted above the non leading term increases with the electron energy; however we can re write the expression (1) in the following form:

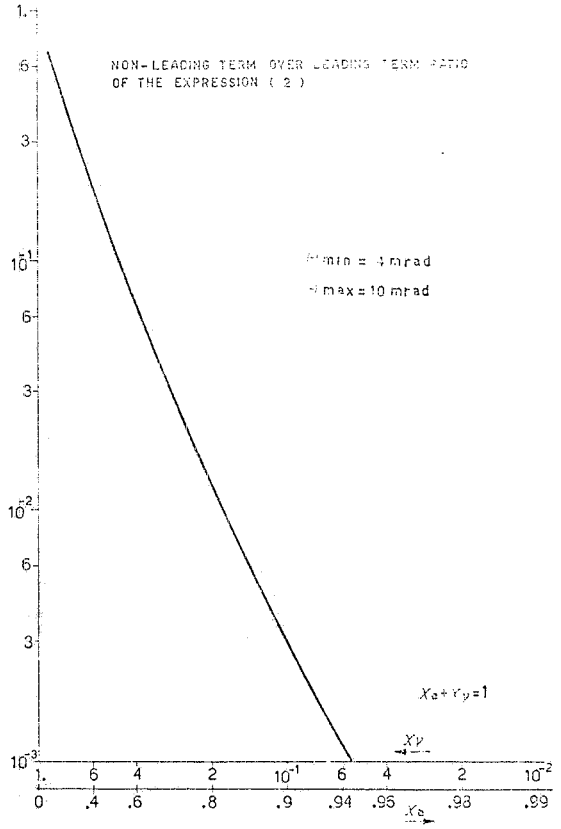

$$N(x_e, \theta_{min}, \theta_{max}) = \frac{\alpha}{\pi(1-x_e)} \cdot \tag{2}$$

$$\cdot \left[\frac{(1+x_e)^2}{4} \ln \frac{(\frac{1-x_e}{\theta_{min}})^2 + x_e}{(\frac{1-x_e}{\theta_{max}})^2 + x_e} + \frac{1}{2} \ln \frac{\theta_{max}}{\theta_{min}} (1-x_e)^2 \right]$$

where the present non leading term $\frac{1}{2} \ln \frac{\theta_{max}}{\theta_{min}}(1-x_e)^2$ now decreases with the electron energy, as one can see in Fig. 2, where the ratio of the non leading term over the leading term is shown versus the electron energy.

The expression (2) neglecting the non leading term can be used with good accuracy starting from $x_e = 0.9$ and it is so much accurated as much the electron energy increases.

FIG. 2 - The non leading term over the leading term ratio of the recoil electron flux emitted in the polar angular range from 4 to 10 mrad.

The single tagging efficiency can be expressed in this way:

$$\varepsilon_{ST} = \frac{\frac{(1+x_e)^2}{4} \ln \frac{(\frac{1-x_e}{\theta_{min}})^2 + x_e}{(\frac{1-x_e}{\theta_{max}})^2 + x_e}}{(1+x_e^2)(\ln \frac{E}{m_e} - \frac{1}{2}) + \frac{(1-x_e)^2}{2}(\ln \frac{2x_e}{1-x_e} + 1) + \frac{(1+x_e)^2}{2} \ln \frac{2x_e}{1+x_e}} = \frac{\ln \frac{(\frac{1-x_e}{\theta_{min}})^2 + x_e}{(\frac{1-x_e}{\theta_{max}})^2 + x_e}}{F(E, x_e)} \tag{3}$$

We now repeat the same already used method: we divide the range $\theta_{min} \div \theta_{max}$ in N parts, putting $\theta_{min} = \theta_1$ and $\theta_{max} = \theta_N$, we can write:

$$\ln \frac{(\frac{1-x_e}{\theta_{min}})^2 + x_e}{(\frac{1-x_e}{\theta_{max}})^2 + x_e} = \sum_{i=2}^{N} \ln \frac{(\frac{1-x_e}{\theta_{i-1}})^2 + x_e}{(\frac{1-x_e}{\theta_i})^2 + x_e}$$

and therefore

$$\varepsilon_{ST} = \sum_{i=2}^{N} \varepsilon_i \tag{4}$$

where

$$\varepsilon_i = \frac{\ln \frac{(\frac{1-x_e}{\theta_{i-1}})^2 + x_e}{(\frac{1-x_e}{\theta_i})^2 + x_e}}{F(E, x_e)}$$

The expression (4) should be right if all recoil electrons emitted with the polar angle θ were effectively detected, but we know that this is not the case for the tagging device behind the low-β quadrupole, where only a fraction f depending on x_e, θ_e and ϕ_e can be detected.

Thus, if f is the detected electron fraction, which is practically constant in the polar angular range $\theta_{i-1} \div \theta_i$, the effective tagging efficiency can be expressed by the formula:

$$\varepsilon_{ST} = \sum_{i=2}^{N} \varepsilon_i f_i \qquad (5)$$

We show in Fig. 3 the detected trajectories fraction versus the electron angle θ_e changes very little for the extreme values of the considered electron energy range; and correspondently in Fig. 4 how the angular acceptances result practically constant in all three cases of low-β quadrupole.

We note that in the standard quadrupole case a "bag" of non zero efficiency appears around $\theta_e \sim 20$ mrad; that is due to electrons emitted around the vertical plane, where a hole is created, it is limited vertically by the converging poles and horizontally by the trigger threshold and the 14 cm limit of the quadrupole gap.

In Fig. 5 the obtained results of the effective tagging efficiency are shown according to the expression (5); in the figure the efficiency curves of the ref. (1) are also presented. These are in very good agreement with the present calculation in the over lapping range $0.9 \div 0.96$ of x_e.

We have stopped our calculation at electron energy $x_e = 0.999$, but of course this method can be used for energies near to 1 so much as one wants.

In Fig. 6 the tagging efficiencies as in Fig. 5 are reported in the whole x_e range from 0.1 to 0.999 and the efficiency of the tagging detector in front to the low-β quadrupole is added covering a polar range from 22 mrad to 300 mrad.

3. - TWO PHOTON MASS SENSITIVITY.

Now we are able to study the two photon mass sensitivity of four tagging system.

The number d^3N of masses in the range $M_x \div M_x + dM_x$ one can produce by two colliding quasi real photons in the energy range $x_{\gamma 1} \div x_{\gamma 1} + dx_{\gamma 1}$ and $x_{\gamma 2} \div x_{\gamma 2} + dx_{\gamma 2}$ respectively can be written in the following way:

$$d^3N = P_1(x_{\gamma 1})\, dx_{\gamma 1}\, P_2(x_{\gamma 2})\, dx_{\gamma 2}\, \delta(M_x^2 - 4E_{beam}^2\, x_{\gamma 1}\, x_{\gamma 2})\, dM_x^2 \qquad (6)$$

where $P_i(x_\gamma)$ $(i = 1, 2)$ represents the probability to have a colliding tagged photon of energy $x_{\gamma 1}$, and it can be defined as:

$$P_i(x_{\gamma i}) = \frac{\int d\phi_e \int d\theta_e\, N_\gamma(x_e, \theta_e, \phi_e)\ \varepsilon_e(x_e, \theta_e, \phi_e)}{\int d\phi_e \int d\theta_e\, N_\gamma(x_e, \theta_e, \phi_e)} \qquad (7)$$

where $\varepsilon_e(x_e, \theta_e, \phi_e)$ is the efficiency to get a recoil electron of energy x_e and polar and azimuthal angle θ_e and ϕ_e respectively, and $N_\gamma(x_e, \theta_e, \phi_e)$ is the photon flux expressed by the corresponding recoil electron parameters.

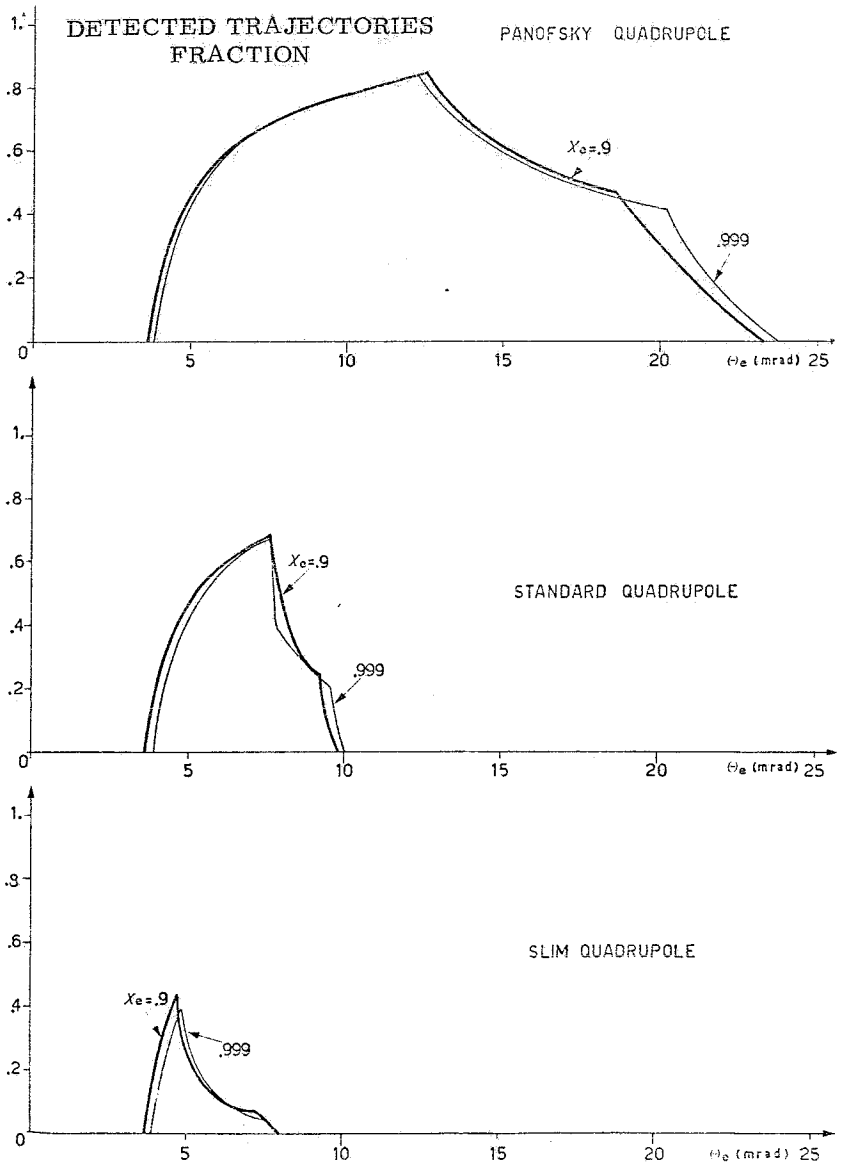

FIG. 3 - Detected Trajectories fraction versus the polar angle for the values of the electron energy of 0.9 and 0.999 times the electron beam energy.

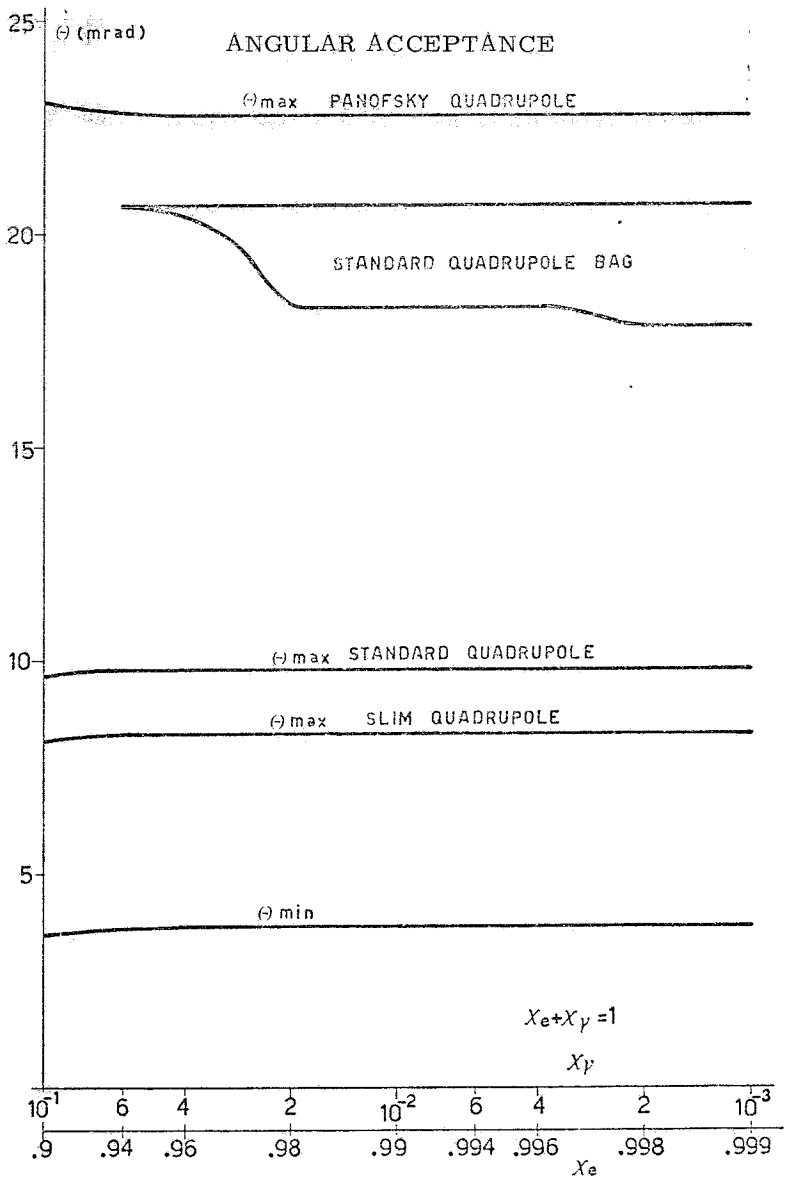

FIG. 4 - Angular acceptances versus the electron energy in the range of x_e from 0.9 to 0.999 for the three kinds of low-β quadrupole.

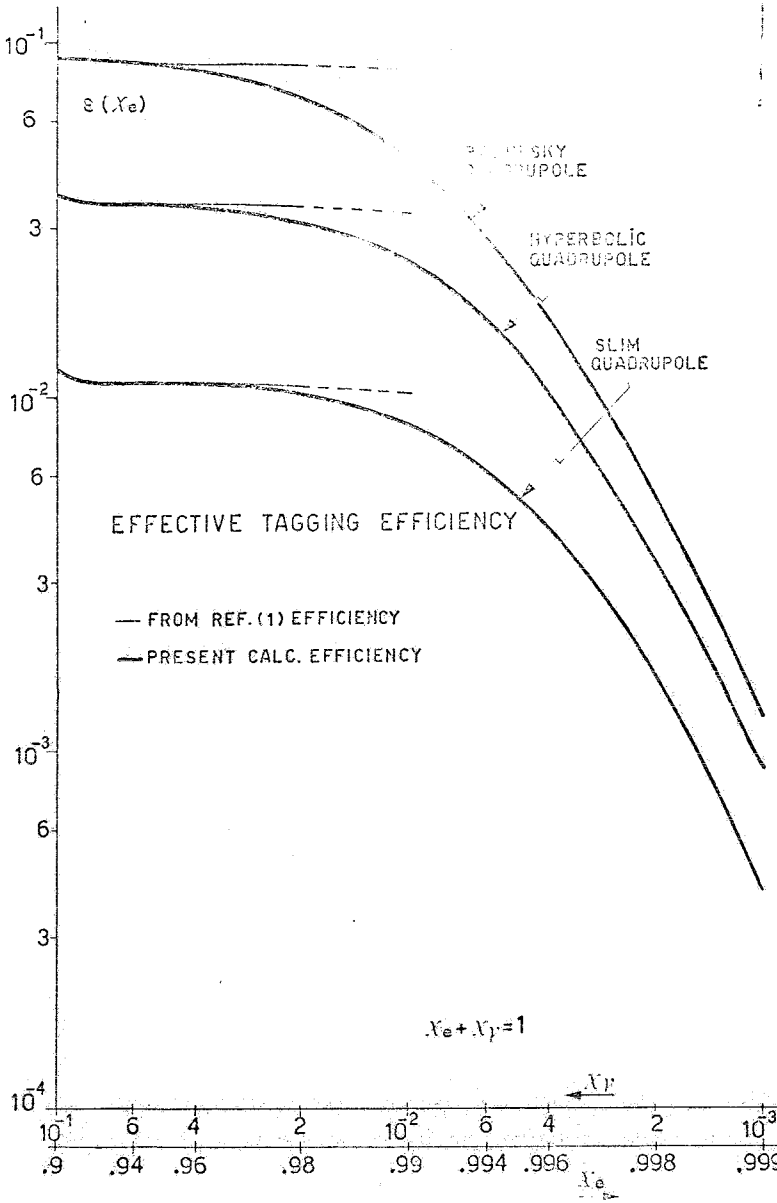

FIG. 5 - Effective tagging efficiencies versus the electron energy in the range from 0.9 to 0.999 for the three kinds of low-β quadrupole.

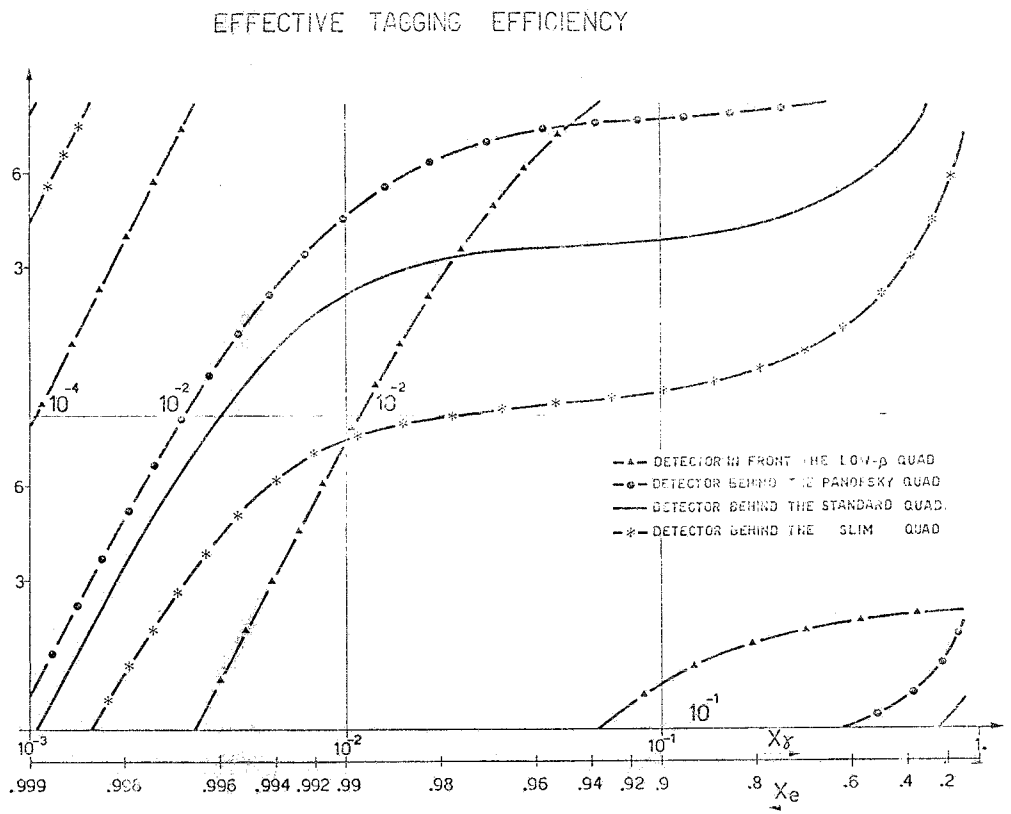

FIG. 6 - Effective tagging efficiencies versus the electron energy in the range from 0.1 to 0.999 for the three kinds of the low-β quadrupole and for the detector in front to the low-β quadrupole covering a θ_e range from 22 to 300 mrad.

We consider our tagging system consisting of two identical arms at both ends of the short insertion (see Fig. 1b).

Each arm is equipped by a tagging detector in front to the low-β quadrupole, we indicate by the symbol IFQPT, covering a polar range from 22 mrad to 300 mrad and the full azimuthal range, and a tagging detector located behind the low-β quadrupole, we indicate by the symbol BQXXT (where XX replaces PN, ST or SL in the case that the low-β quadrupole is the Panofsky, the standard or the "slim" quadrupole respectively).

Now for the IFQPT detector the efficiency is defined as it follows:

$$\varepsilon_e(x_e, \theta_e) = 1 \qquad \text{if} \qquad \theta_{min} < \theta_e < \theta_{max}$$

$$\varepsilon_e(x_e, \theta_e) = 0 \qquad \text{if} \qquad \theta_e < \theta_{min} \quad \text{or} \quad \theta_e > \theta_{max}$$

for all azimuthal angles.

Then the expression (7) becomes:

$$P_i(x_{\gamma i}) = \frac{N_e(x_e, \theta_{min}, \theta_{max})}{N_e(x_e, \theta_{min} = 0, \theta_{max} = \pi)} \tag{8}$$

where the quantities at numerator and denominator of the ratio in (8) represent the electron flux emitted in the polar range $\theta_{min} \div \theta_{max}$. So $P_i(x_\gamma)$ is the IFQPT detector efficiency we call $\varepsilon^F_{ei}(x_\gamma)$. For the BQXXT detector the expression (7) coincides with the single tagging efficiency of the expression (5):

$$P_i(x_{\gamma i}) = \sum_{i=2}^{N} \varepsilon_i f_i \tag{9}$$

where the integration on θ_e and ϕ_e has been performed by means a suitable summation; therefore $P_i(x_{\gamma i})$ represents the BQXXT detector efficiency we call $\varepsilon^B_{ei}(x_{\gamma i})$.

Putting for brevity sake

$$\varepsilon_{ei}(x_{\gamma i}) = \varepsilon^F_{ei}(x_{\gamma i}) + \varepsilon^B_{ei}(x_{\gamma i})$$

the expression (6) can be rewritten, taking into account the kinematical relation: $x_{ei} + x_{\gamma i} = 1$:

$$d^3N = \varepsilon_{e1}(1-x_{\gamma 1})\, \varepsilon_{e2}(1-x_{\gamma 2})\, \delta(M_x^2 - 4E^2_{beam} x_{\gamma 1} x_{\gamma 2})\, dx_{\gamma 1}\, dx_{\gamma 2}\, dM_x^2 \tag{10}$$

Performing an integration on the $x_{\gamma 2}$ variable we get:

$$d^2N = \varepsilon_{e1}(1-x_\gamma)\, \varepsilon_{e2}(1-\frac{k}{x_\gamma})\, \frac{dx_\gamma}{x_\gamma}\, \frac{dM_x^2}{4E^2_{beam}} \tag{11}$$

where $k = (M_x/2E_{beam})^2$ and by the symmetry between $x_{\gamma 1}$ and $x_{\gamma 2}$ it isn't necessary to keep yet the index in x_γ. So the quantity

$$\frac{d^2N}{dM_x^2\, dx_\gamma} = \frac{\varepsilon_{e1}(1-x_\gamma)\, \varepsilon_{e2}(1-\frac{k}{x_\gamma})}{4E^2_{beam}\, x_\gamma} \tag{12}$$

represents the number of collisions where a mass M_x is produced by two tagged photons.

Now since by the quantity

$$\left(\frac{d^2N}{dM_x^2 x_\gamma}\right)_{\varepsilon_{e1} = \varepsilon_{e2} = 1}$$

we indicate the number of all collisions where a mass M_x is produced, the detection efficiency $\varepsilon(M_x, x_\gamma)$ to get a mass M_x can be defined:

$$\varepsilon(M_x, x_\gamma) = \frac{\dfrac{d^2N}{dM_x^2 dx_\gamma}}{\left(\dfrac{d^2N}{dM_x^2 dx_\gamma}\right)_{\varepsilon_{e1} = \varepsilon_{e2} = 1}} = \varepsilon_{e1}(1-x_\gamma)\ \varepsilon_{e2}\left(1-\frac{k}{x_\gamma}\right) \qquad (13)$$

Results of the expression (13) are plotted from Fig. 7 to Fig. 13 for six values of the M_x mass: 5, 10, 30, 60, 90 and 120 GeV/c^2 and for an electron beam energy of 80 GeV.

The Fig. 7 corresponds to the case where one uses only the IFQPT detector ($\varepsilon^F_{ei} \neq 0$, $\varepsilon^B_{ei} = 0$) and Figs. 8, 9 and 10 to the case where one uses only the BQXXT detector ($\varepsilon^F_{ei} = 0$, $\varepsilon^B_{ei} \neq 0$), while the Figs. 11, 12 and 13 shows results of both operating detectors ($\varepsilon^F_{ei} \neq 0$, $\varepsilon^B_{ei} \neq 0$) in the three choices of the low-β quadrupole.

These results show that tha efficiency $\varepsilon(M_x, x_\gamma)$ is a falling function of the photon energy in the lower mass region and a constant one in the higher mass region in the IFQPT detector case.

In the BQXXT detector cases the $\varepsilon(M_x, x_\gamma)$ is less falling in the lower mass region and it is an increasing function in the higher mass region.

However it is more significant to present these results through the efficiency to get a mass M_x by whatever photon energy x_γ it is created; in other words we define the two photon mass sensitivity of four tagging system like an efficiency $\varepsilon(M_x)$, which can be expressed like that:

$$\frac{\displaystyle\int_{\sqrt{k}}^{0.9} dx_\gamma \left(\frac{d^2N}{dM_x^2 dx_\gamma}\right)}{\displaystyle\int_{\sqrt{k}}^{0.9} dx_\gamma \left(\frac{d^2N}{dM_x^2 dx_\gamma}\right)_{\varepsilon_{e1} = \varepsilon_{e2} = 1}} = \frac{\displaystyle\int_{\sqrt{k}}^{0.9} \frac{dx_\gamma}{x_\gamma}\ \varepsilon_{e1}(1-x_\gamma)\ \varepsilon_{e2}\left(1-\frac{k}{x_\gamma}\right)}{\displaystyle\int_{\sqrt{k}}^{0.9} \frac{dx_\gamma}{x_\gamma}} \qquad (14)$$

The results of mass sensitivity from the expression (14) are shown in Fig. 14 in the seven cases of possible choices we have mentioned above.

In general the function $\varepsilon(M_x)$ appears to be fast rising in the mass region below 10 GeV/c^2, while after that value it rises rather smoothly.

The IFQPT detector behaviour is rather different in respect to that of the BQXXT detector; for istance at 10 GeV/c^2 the mass efficiency is the same for the IFQPT and BQPNT detector, however for lower masses the BQPNT efficiency is larger thah that of the IFQPT and for higher masses it happens just the contrary.

As far as the coupled use of both tagging detectors is concerned it seems that the choice of the Panofsky quadrupole provides no more that about a factor of two in respect to the standard quadrupole case. The high cost of the Panofsky quadrupole should forbid such a choice.

The case of the "slim" quadrupole could be rather interesting, because in spite to a lower mass sensitivity in respect to the standard quadrupole, that choice allows to set up a high class IFQPT detector using the recovered space around it.

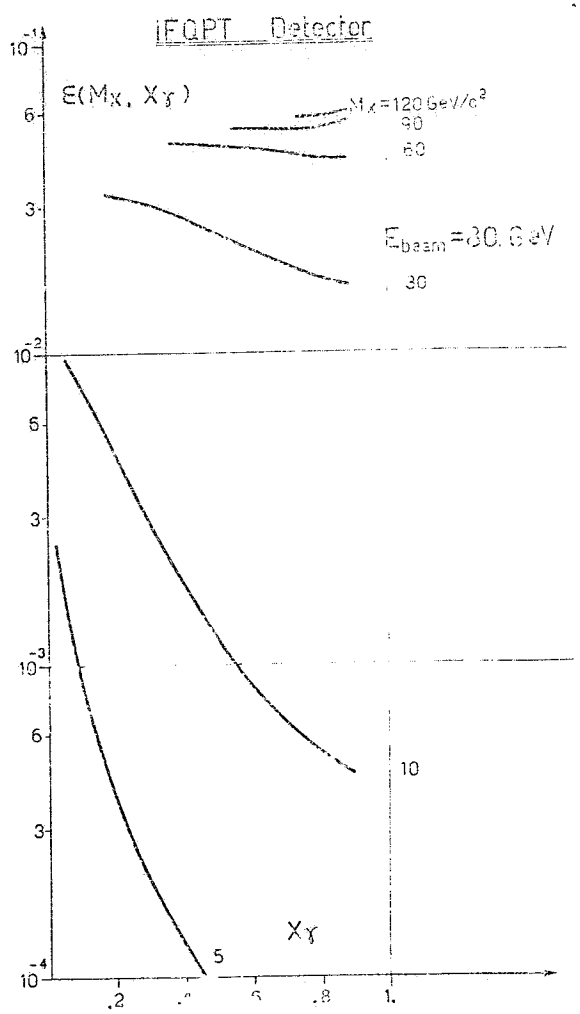

FIG. 7 - The two photon mass efficiency of the IFQPT detector versus the photon energy for six fixed values of M_X.

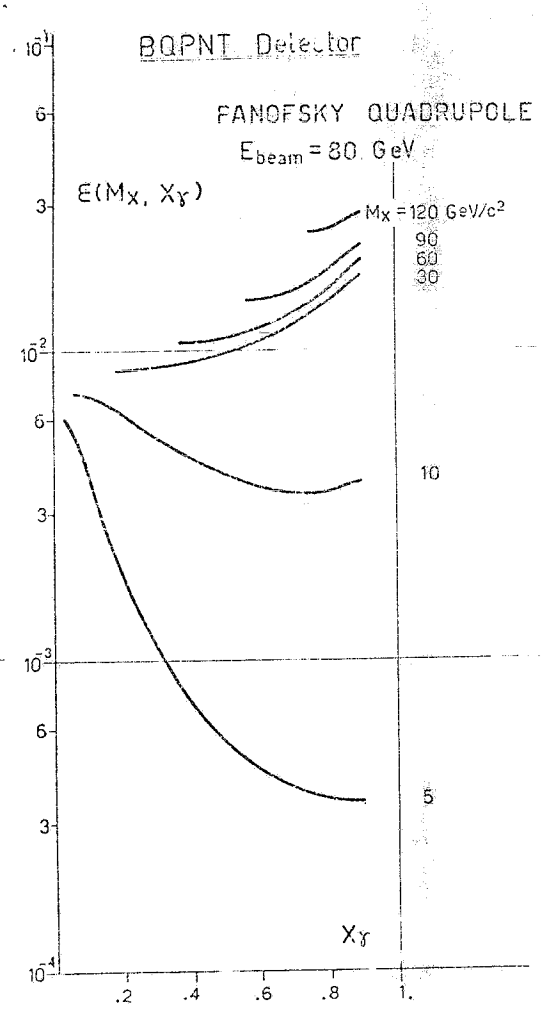

FIG. 8 - The two photon mass efficiency of the BQPNT detector versus the photon energy for six fixed values of M_X.

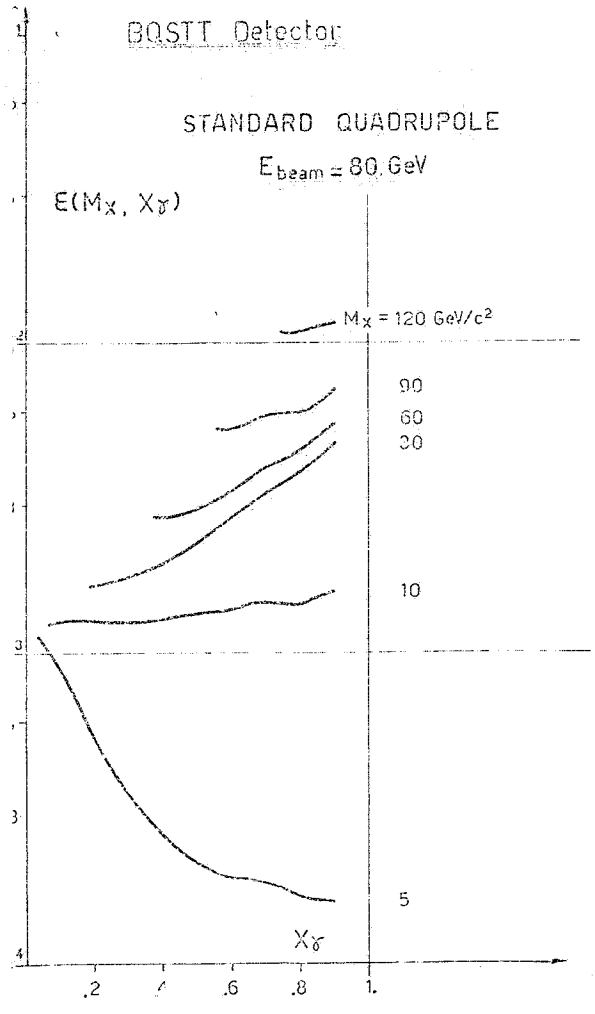

FIG. 9 - The two photon mass efficiency of the BQSTT detector versus the photon energy for six fixed values of M_X.

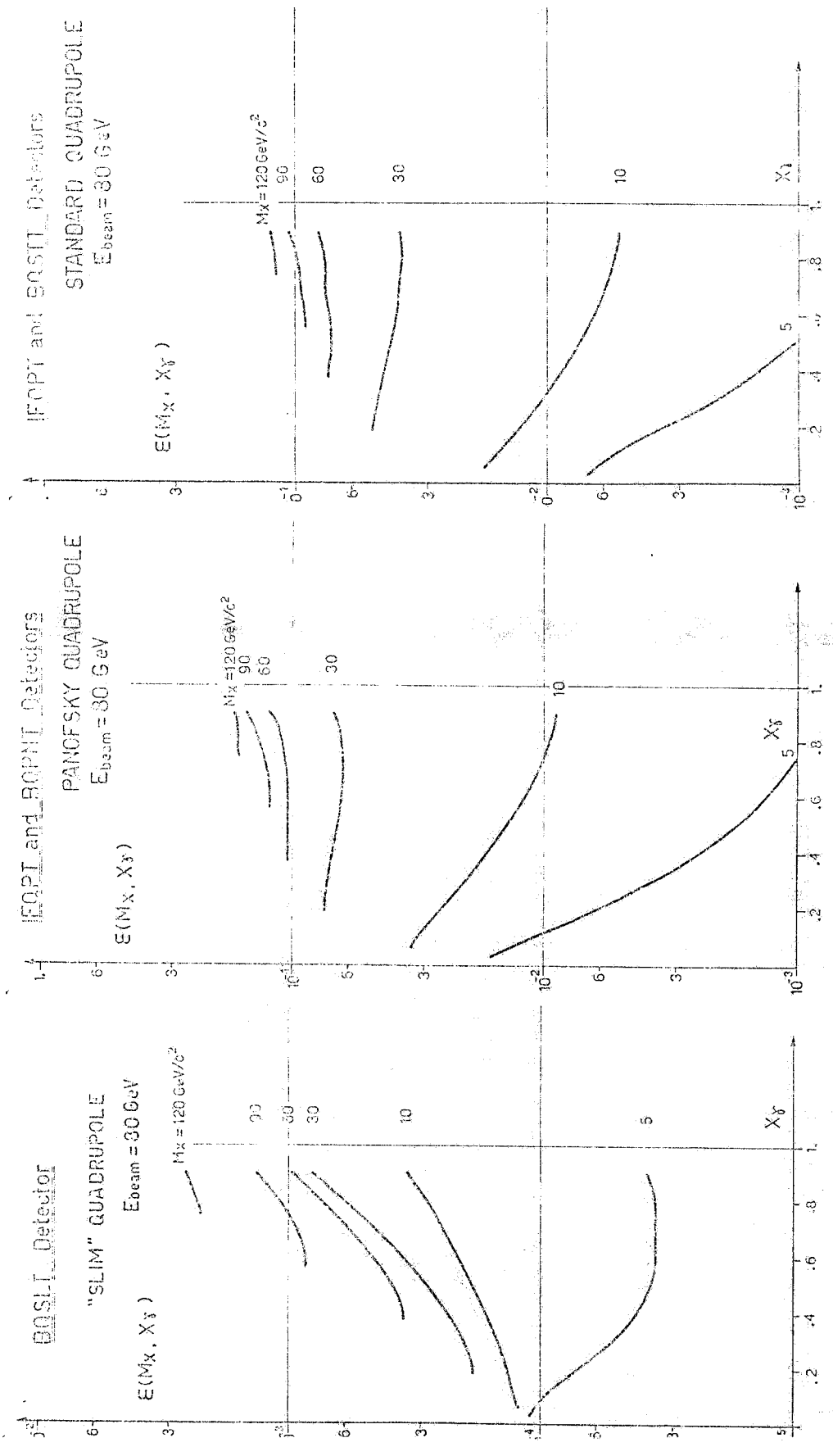

FIG. 10 - The two photon mass efficiency of the BQSLT detector versus the photon energy for six fixed values of M_X.

FIG. 11 - The two photon mass efficiency of both IFQPT and BQPNT detectors versus the photon energy for six fixed values of M_X.

FIG. 12 - The two photon mass efficiency of both IFQPT and BQSTT detectors versus the photon energy for six fixed values of M_X.

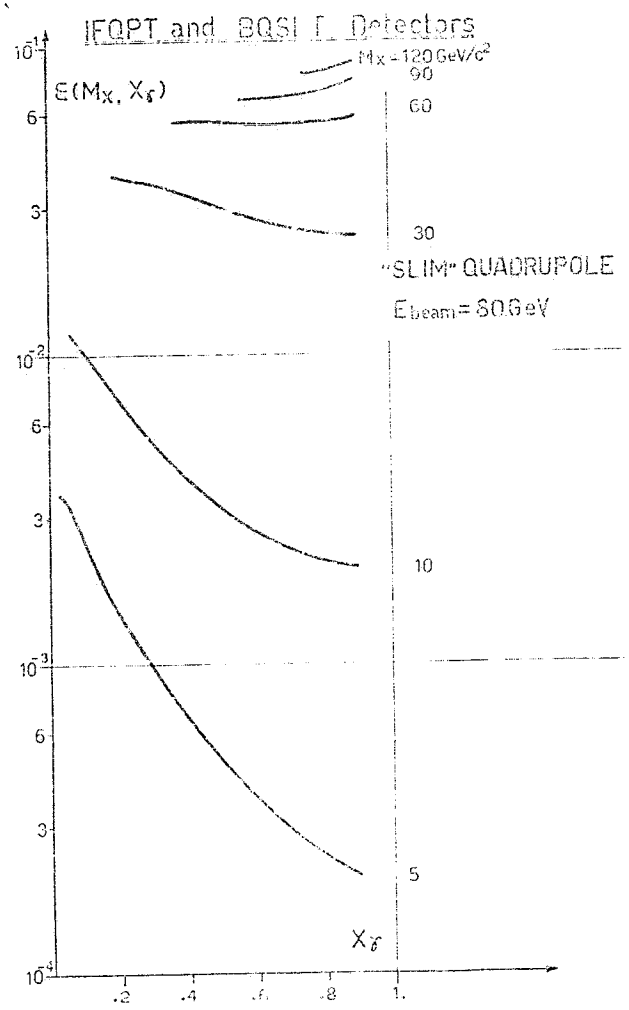

FIG. 13 - The two photon mass efficiency of both IFQPT and BQSLT detectors versus the photon energy for six fixed values of M_X.

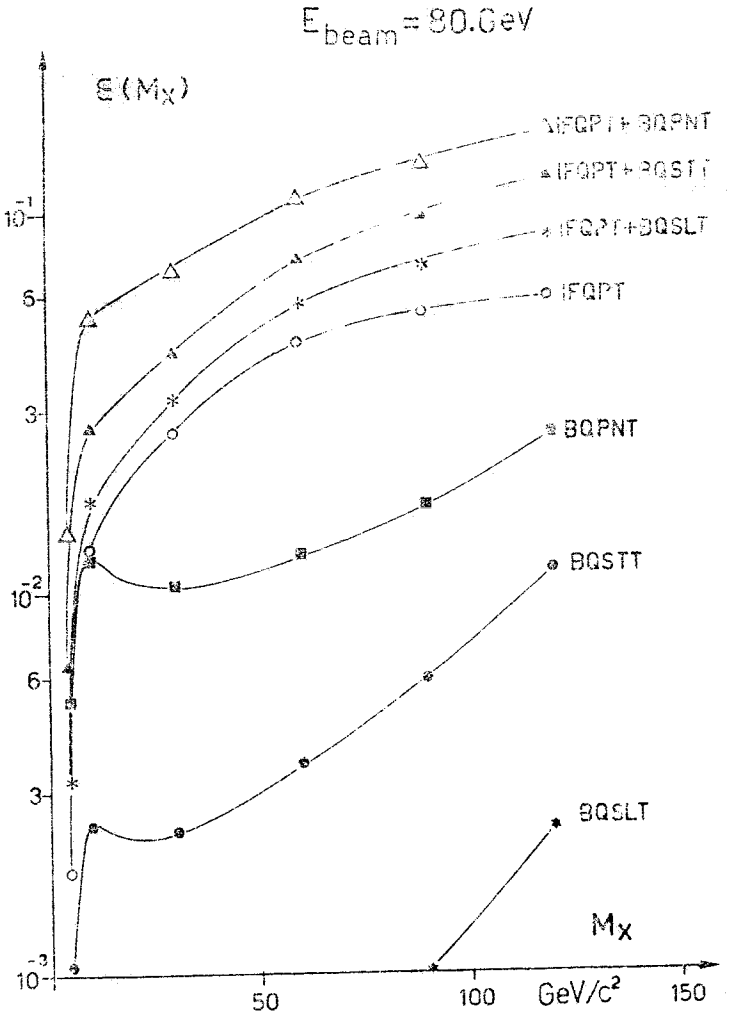

FIG. 14 - The two photon mass efficiency versus M_X for seven possible configurations of the IFQPT and BQXXT detectors.

4. - SHAPE ASPECTS OF THE TAGGING DETECTOR BEHIND THE LOW-β QUADRUPOLE.

In this section we want to give more diffuse details than those already given in the ref. (1) on the angular acceptances one can reach by a tagging detector behind the low-β quadrupole.

In fact we think that it will be useful for a tagging detector design to know where the electron fluxes of the accepted angular regions are located and how these fluxes depend on the kind of low-β quadrupole one uses.

We show some regions in the plane of the polar angle θ_e and the azimuthal angle ϕ_e, for a fixed electron energy, and relatively to the first quadrant in the angle ϕ_e (the accepted regions in the other quadrant are simply obtained by the symmetry property in respect to the quadrupolar axes).

The points inside these regions have the proper θ_e, ϕ_e and x_e value so that the corresponding electron is a "detectable" electron, i. e. it doesn't hit thick material and crosses the transverse plane 2.5 meters far from the low-β quadrupole and at a distance from the circulating beam larger than 9 cm.

We show how these accepted regions are modified at different energies, in fact we present three regions corresponding at an electron energy of 0.3, 0.6 and 0.9 times the electron beam energy.

In Figs. 15, 16 and 17 we report the acceptance regions corresponding respectively to the Panofsky quadrupole, the standard quadrupole and the "slim" quadrupole cases.

It is interesting to investigate how these fluxes corresponding to those regions are located behind the quadrupole, in fact that is directly connected to the geometry of the detector one may set up.

At this end we think that it is representative to give the "projection" of the accepted angular regions on the crossing planes located in the positions "A" and "B" of the Fig. 1b.

In the Figs. 18, 19 and 20 we give the projected regions corresponding to the Figs. 15, 16 and 17 in the crossing plane located in the position "A" and in the Figs. 21, 22 and 23 the same projections in the crossing plane located in the position "B".

We note that the electron fluxes coming from the first quadrant can hit possibly the crossing plane located in "B" at negative vertical values, since the focal vertical length becomes shorter as the electron energy decreases.

As general remark we observe that the radial size of a possible detector depends strongly on the kind of quadrupole one uses, and the vertical size is connected to how small one puts the lower limit of the electron energy acceptance.

In any case the detector appears to get a shape radially disposed.

REFERENCE.

(1) - R. Del Fabbro and G. P. Murtas, Tagging systems at LEP short insertion: angular acceptances and efficiencies, ECFA/LEP Working Group SSG/6/2/March 1979, Frascati report LNF-79/23 (1979).

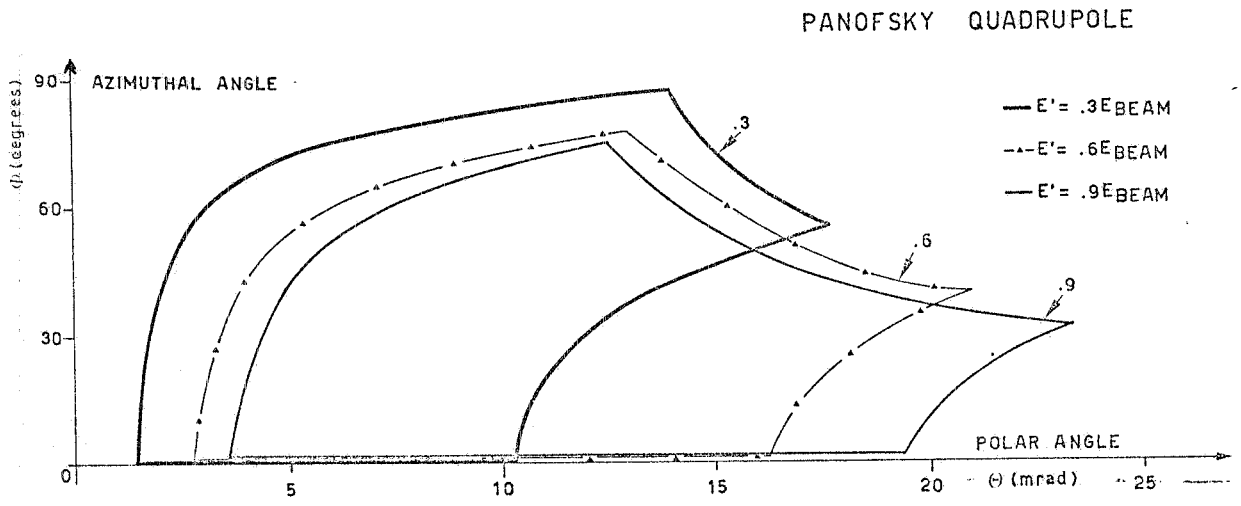

FIG. 15 - Nonzero efficiency regions in the polar-azimuthal angle plane for three fixed values of electron energy in the Panofsky quadrupole plane.

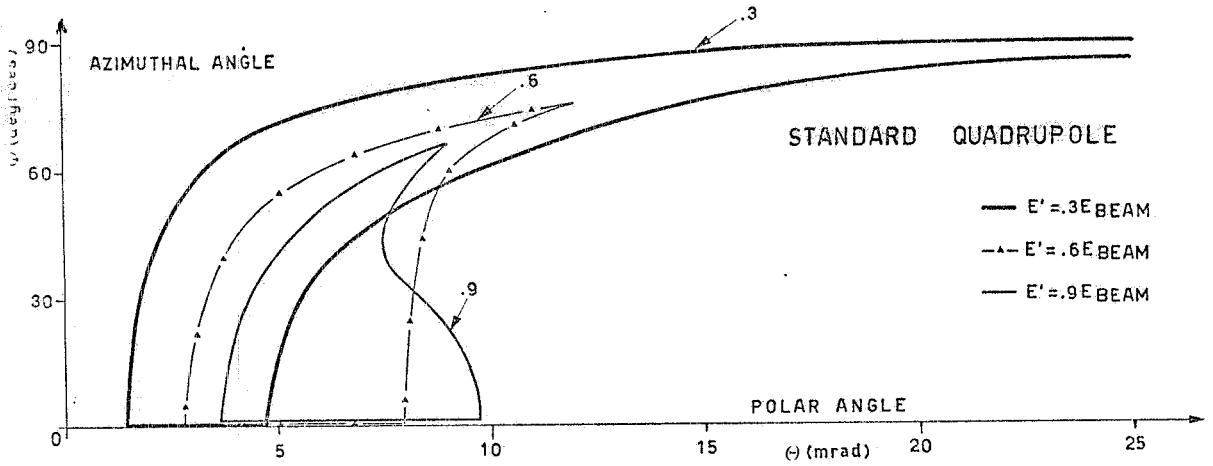

FIG. 16 - Nonzero efficiency regions in the polar-azimuthal angle plane for three fixed values of the electron energy in the standard quadrupole case.

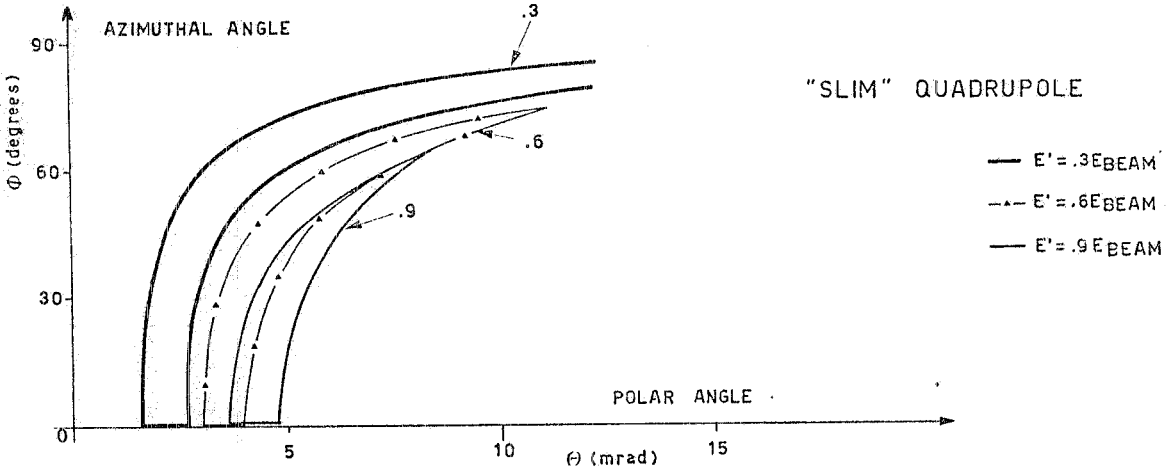

FIG. 17 - Nonzero efficiency regions in the polar-azimuthal angle plane for three fixed values of the electron energy in the "slim" quadrupole case.

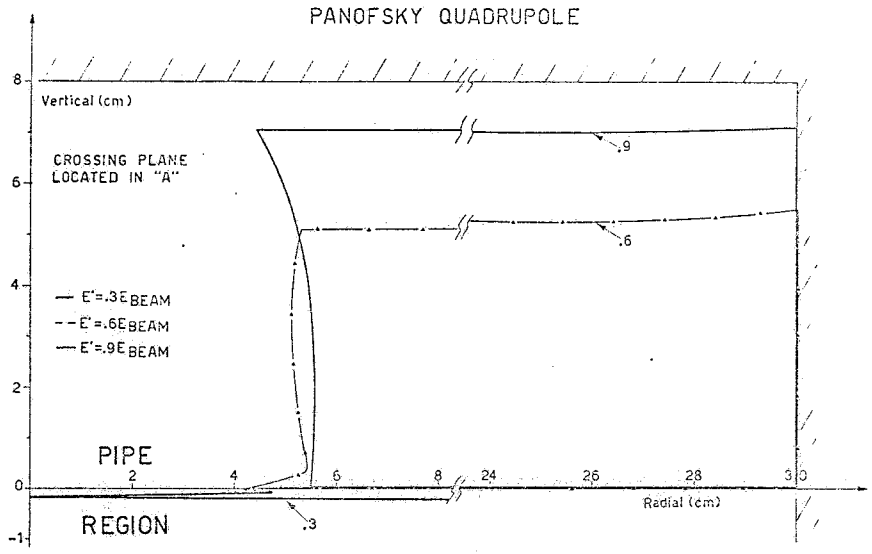

FIG. 18 - Pattern of the detected electron flux by the crossing with the vertical plane in the position "A" for three fixed values of the electron energy in the Panofsky quadrupole case.

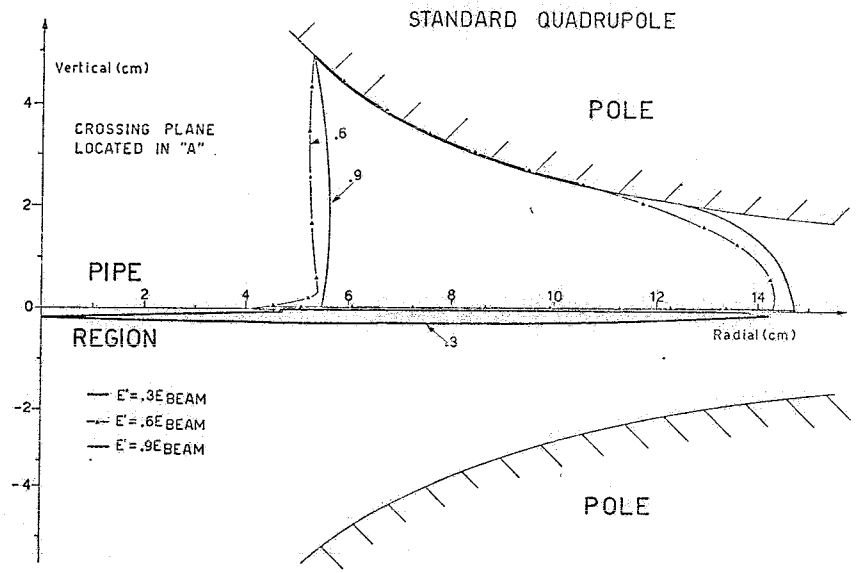

FIG. 19 - Pattern of the detected electron flux by the crossing with the vertical plane in the position "A" for three fixed values of the electron energy in the standard quadrupole case.

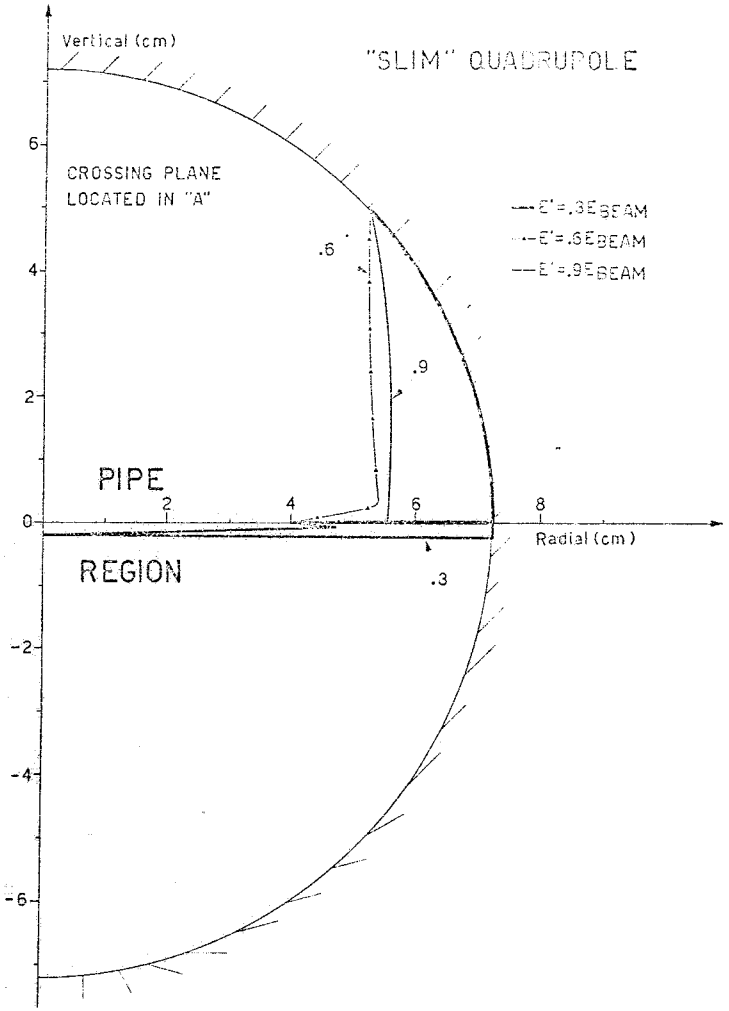

FIG. 20 - Pattern of the detected electron flux by the crossing with the vertical plane in the position "A" for three fixed values of the electron energy in the "slim" quadrupole case.

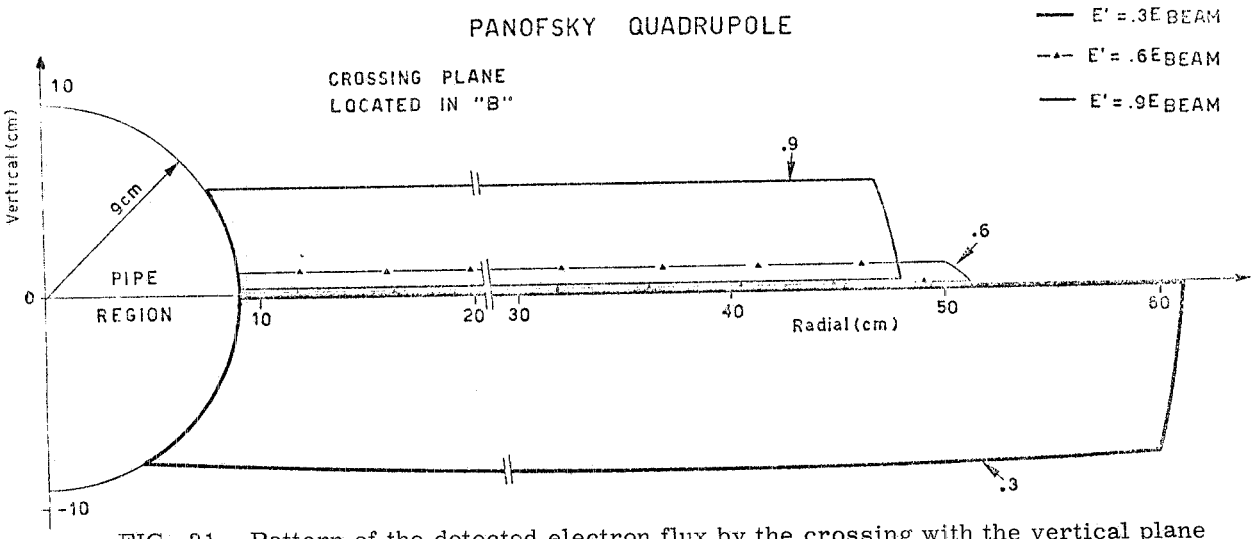

FIG. 21 - Pattern of the detected electron flux by the crossing with the vertical plane in the position "B" for three fixed values of the electron energy in the Panofsky quadrupole case.

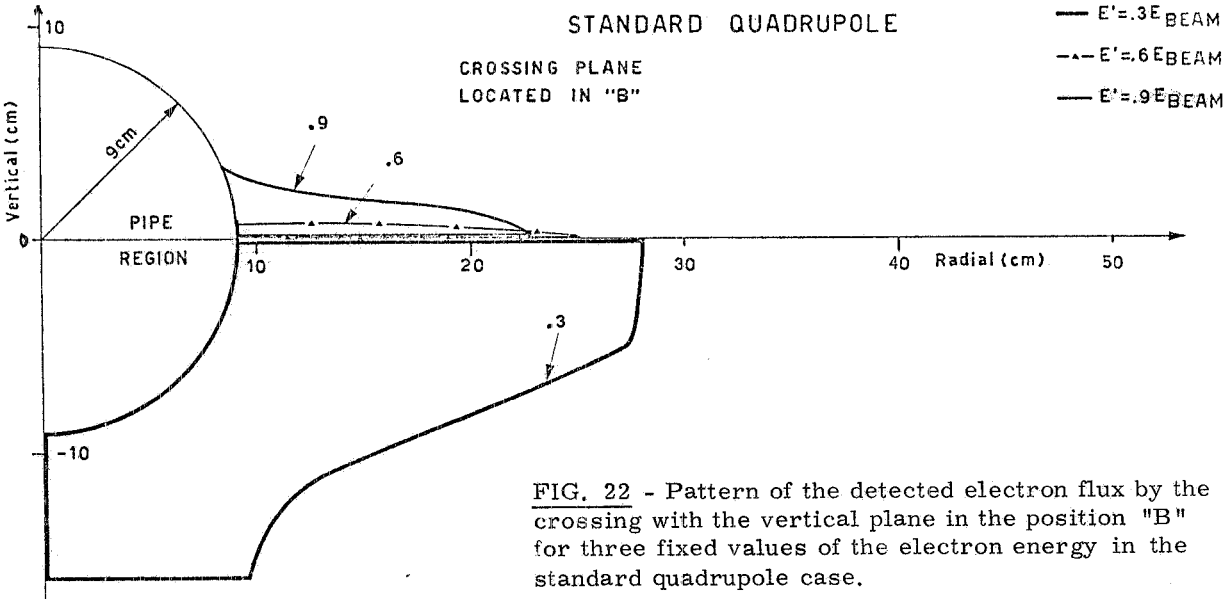

FIG. 22 - Pattern of the detected electron flux by the crossing with the vertical plane in the position "B" for three fixed values of the electron energy in the standard quadrupole case.

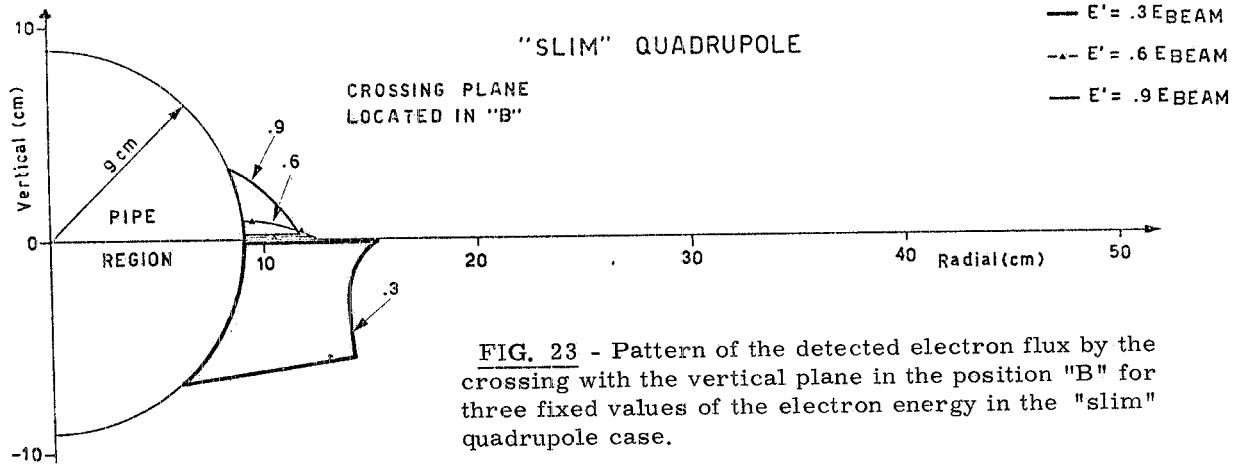

FIG. 23 - Pattern of the detected electron flux by the crossing with the vertical plane in the position "B" for three fixed values of the electron energy in the "slim" quadrupole case.

CURRENT LNF PREPRINTS AND REPORTS

LNF-79/32(P) F. Balestra, M. P. Bussa, L. Busso, I. V. Falomkin, R. Garfagnini, C. Guaraldo, A. Maggiora, G. Piragino, G. B. Pontecorvo, R. Scrimaglio and Yu. A. Shcherbakov:
π^+ MESONS INTERACTION ON ^{4}He AT 120, 145 AND 165 MeV
(Submitted to Nuclear Physics A).

LNF-79/33(P) C. Bacci, R. Baldini Celio, G. Capon, R. Del Fabbro, P. De Santis, G. De Zorzi, M. Grilli, E. Iarocci, C. Mencuccini, G. P. Murtas, G. Penso, M. Spinetti, B. Stella and V. Valente:
EXPERIMENTAL RESULTS ON PHOTON-PHOTON INTERACTIONS AT ADONE
(Submitted to Physics Letters).

LNF-79/34(P) C. Bacci, R. Baldini Celio, G. Battistoni, D. Bollini, G. Capon, R. Del Fabbro, G. De Zorzi, E. Iarocci, M. M. Massai, S. Moriggi, G. P. Murtas, G. Panso, M. Spinetti, B. Stella and L. Trasatti:
TOTAL CROSS SECTION FOR HADRONIC PRODUCTION BY e^+e^- ANNIHILATION IN THE TOTAL C. M. ENERGY RANGE 1.42-3.09 GeV
(Submitted to Physics Letters).

LNF-79/35(R) P. Spillantini:
AZIMUTHAL DISTORTION AND SPIRALLING OF CHARGED PARTICLES IN A SOLENOID AT LEP.

LNF-79/36(P) G. Bologna, F. Celani, A. Codino, B. D'Ettorre Piazzoli, F. L. Fabbri, G. Levy, G. Mannocchi, P. Picchi, G. Rivellini, G. Satta, P. Spillantini and A. Zallo:
A REMOTELY PROGRAMMABLE SYSTEM TO SUPPLY CONTROL AND DISPLAY NEGATIVE HIGH VOLTAGE OF MULTIWIRE AND DRIFT CHAMBERS
(To be submitted to Nuclear Instrument and Methods).

LNF-79/37(P) G. De Franceschi and F. Palumbo:
SPONTANEOUS SUPERSYMMETRY BREAKING AND SUPERCONDUCTIVITY IN A NONRELATIVISTIC MODEL
(Submitted to Nuclear Physics B).

LNF-79/38(P) G. Parisi:
THE ORDER PARAMETER FOR SPIN GLASSES: A FUNCTION ON THE INTERVAL 0-1
(To be submitted to Journal of Physics A).

LNF-79/39(P) G. Curci, M. Greco, Y. Srivastava and B. Stella:
QCD ANALYSIS OF JET LONGITUDINAL MOMENTA
(Submitted to Physics Letters B).

AVAILABLE FROM (It is not necessary to write to the authors):

Servizio Documentazione
INFN - Laboratori Nazionali di Frascati
Casella Postale 13
00044 FRASCATI (Italy).